Low Temperature Physics/Fizika Nizkikh Temperatur, 2014, v. 40, No. 10, pp. 1155–1160

Mechanisms of normal reflection at metal interfaces studied by Andreev-reflection spectroscopy

K. Gloos

Wihuri Physical Laboratory, Department of Physics and Astronomy, University of Turku, FIN-20014 Turku, Finland

Turku University Centre for Materials and Surfaces (MatSurf), FIN-20014 Turku, Finland
E-mail: kgloos@utu.fi

E. Tuuli

Wihuri Physical Laboratory, Department of Physics and Astronomy, University of Turku, FIN-20014 Turku, Finland

The National Doctoral Programme in Nanoscience (NGS-NANO), FIN-40014 University of Jyväskylä, Finland

Received May 22, 2014, published online August 21, 2014

Andreev-reflection spectroscopy of elemental superconductors in contact with nonmagnetic normal metals reveals that the strength of normal-reflection varies only slightly. This observation imposes strong constrictions on the three possible normal-reflection mechanisms: tunneling through a dielectric barrier, reflection due to the different electronic properties of the two electrodes, and diffusive transport caused by elastic scattering in the contact region. We discuss in detail the role played by Fermi-surface mismatch, represented by the different Fermi velocities on both sides of the contact interface. We find that it is at least not the dominant mechanism and possibly completely absent in the Andreev-reflection process.

PACS: 85.30.Hi Surface barrier, boundary, and point-contact devices;
73.40.–c Electronic transport in interface structures;
74.45.+c Proximity effects; Andreev reflection; SN and SNS junctions.

Keywords: point contacts, metal interfaces, normal reflection, Andreev reflection.

1. Introduction

How do electrons cross a direct interface between a normal and a superconducting metal? At a tunnel junction the superconducting gap suppresses electron transport at small energies around the Fermi level. At a direct contact with no or only a very weak tunneling barrier, Andreev reflection transfers an additional electron for each incident one to form a Cooper pair in the superconductor. In an alternative picture the Cooper pair is composed of the incident electron plus a newly created one by emitting a hole. Because of energy and momentum conservation this hole travels back through the contact and into the normal conductor along almost the same path taken by the incident electron. Normal reflection as the natural counter part of Andreev reflection enhances the interface resistance, normal reflection of the second electron or the retro-reflected hole creates the characteristic double-minimum structure of the Andreev-reflection resistance spectra. While the role of Andreev reflection in the transport process across the interface is understood [1], the normal-reflection part is far from being settled.

Normal reflection at a metal interface reduces its transmission coefficient $\tau = 1/(1+Z^2)$ to below unity. The dimensionless Z parameter represents the strength of a δ-function tunneling barrier that approximates a more realistic rectangular barrier of finite height Φ and width w according to $Z_\delta = \Phi w/\hbar v_F$ for electrons with (average) Fermi velocity v_F [1]. Two other mechanisms contribute to normal reflection. First, Fermi-surface mismatch, again in terms of a δ-function barrier, adds $Z_{FSM} = |1-r|/(2\sqrt{r})$, where $r = v_{F1}/v_{F2}$ is the ratio of Fermi velocities of the two electrodes [2]. Second, diffusive transport through the contact region conserves electron and hole energies in elastic scattering processes, but not their momentum. This allows partial backscattering of the incident electron as well as the second electron or the retro-reflected hole. A diffusive contact is thought to consist of a certain number of modes, each mode i has its own transmission coefficient τ_i. An ideal long diffusive junc-

tion has a distribution of transmission coefficients which sums up to a single $Z_{\rm diff} \approx 0.55$ [3,4].

Real contacts could have any combination of those three mechanisms. Unless one of them dominates, separating the different contributions requires that they do not depend on each other, for example when the tunneling barrier sits at the end of the diffusive channel, or on one side of the interface and not on the other, with the total $Z \approx \sqrt{Z_{\rm diff}^2 + Z_{FSM}^2 + Z_\delta^2}$. Real contacts are probably more intricate than described by a δ-function barrier [2,5]. However, before invoking more involved and speculative modelling, one should try to explain the experimental data by starting with the most basic mechanisms mentioned above.

Naidyuk *et al.* [6] as well as Naidyuk and Yanson [7] have noticed that S (superconducting)–N (normal) point contacts, including those with unconventional heavy-fermion and high-temperature superconductors, often have Z parameters between 0.4 and 0.5, and that those contacts could be in the diffusive limit. During the last couple of years we have found similar $Z \approx 0.5$ values for many S–N combinations over a wide range of contact resistances or lateral contact sizes that can not be explained by a dielectric barrier [8–10]. Since point contacts between conventional metals and heavy-fermion compounds with up to two orders of magnitude smaller v_F also have $Z \approx 0.4-0.5$ [7], Fermi-velocity mismatch does not seem to be a valid approach. That is why our initial interpretation of point-contact experiments with superconducting niobium and conventional metals [8], which we will revise here, was based on the mismatch of Fermi momentum. Additionally, niobium provides such a wide margin of possible Fermi wave numbers from less than 4 $\rm nm^{-1}$ up to 22 $\rm nm^{-1}$ that one can almost freely pick a suitable one [8].

We show here by comparing Andreev-reflection data of contacts between elemental superconductors and nonmagnetic normal metals that Fermi-surface mismatch is not the dominant mechanism of normal reflection. Moreover, we suggest that even theoretically Fermi-surface mismatch does not affect normal reflection of the Andreev-reflected holes.

2. Experiments and results

We fabricated the point-contact interfaces using the shear (crossed wire) method by moving the two sample wires towards each other until they touch at one spot [11]. Before the contact is set, the wires slide against each other and, thus, either remove or break up possible remains of an oxide layer, improving the chance that the contacts are formed between relatively clean surfaces. The normal conductors were silver (Ag), gold (Au), copper (Cu), palladium (Pd), and platinum (Pt), and the superconductors aluminum (Al, T_c = 1.2 K), cadmium (Cd, 0.56 K), indium (In, 3.4 K), niobium (Nb, 9.2 K), tantalum (Ta, 4.4 K), tin (Sn, 3.7 K), titanium (Ti, 0.5 K), and zinc (Zn, 0.87 K). The wires had a diameter of 0.25 mm except Al (0.5 mm), Cd (1.0 mm), and In (1.5 mm). Surface treatment did not noticeably affect the spectra with two exceptions that had otherwise enhanced Z values or stronger normal reflection. The oxide layer of Nb was removed using fine abrasive paper, and that of Zn by dipping the wire in dilute HCl acid. Before installing and cooling down, the wires were cleaned in an ethanol ultrasound bath.

The contacts were measured in the vacuum region of a dilution refrigerator. A dc current I with a small superposed ac component dI ran through the contact, and the voltage drop $V + dV$ across the contact was measured to obtain the $I(V)$ characteristics as well as the differential resistance spectrum $dV/dI(V)$. In addition to S–N contacts we have also investigated S_1–S_2 junctions between two different superconductors S_1 and S_2 that had critical temperatures $T_{c1} \gg T_{c2}$, for example Nb–Al or In–Zn, above T_{c2} to drive superconductor S_2 normal while S_1 still remains superconducting. Strong superconductors S_1 = In, Ta, and Nb needed temperatures well above T_{c2} to suppress proximity-induced superconductivity in S_2. The spectra were fitted using the modified BTK theory [12,13] that includes Dynes' lifetime parameter Γ [14]. This model contains only two other adjustable parameters, the energy gap 2Δ and the Z parameter. The differential resistance at large bias voltages coincided with the normal contact resistance R_N. Not all contacts revealed the typical Andreev-like spectra that could be easily analyzed, but had additional anomalies. Find examples for the distribution between "good" and "bad" contacts in Ref. 10.

Figure 1 shows representative spectra of a Zn–Ag contact as function of temperature together with the fit parameters. The energy gap $2\Delta(T)$ follows closely the theoretical BCS curve [15], while $Z(T)$ and $\Gamma(T)$ barely depend on temperature. The Z parameter could be determined within $\Delta Z \approx \pm 0.01$ when the Andreev-reflection double-minimum structure is visible. Near T_c we kept Z constant and adjusted only 2Δ and Γ.

Figures 2–5 show the Z parameters as function of contact resistance R_N for various S–N combinations. Note that in many cases from small resistances of less than 1 Ω (contact diameter ≈ 30 nm) to above 1 kΩ (contact diameter ≈ 1 nm) the Z parameter stays rather constant at around 0.5. At higher resistances above 1 kΩ the contacts typically had larger Z values, probably because small interface areas are more susceptible to the surface quality. Also the cleaning mechanism of the shear contacts does not seem to work well with a soft counter electrode like In as shown in Fig. 2(c) where some of the In–Zn contacts had large Z already at small R_N. Some of the Al contacts in Fig. 3 had Z down to 0.3 in the $R_N \approx 100-1000$ Ω range [9]. Since this was accompanied by enhanced 2Δ and Γ, we suspect that those small Z values could be artefacts caused by inhomogeneous superconductivity in the contact region.

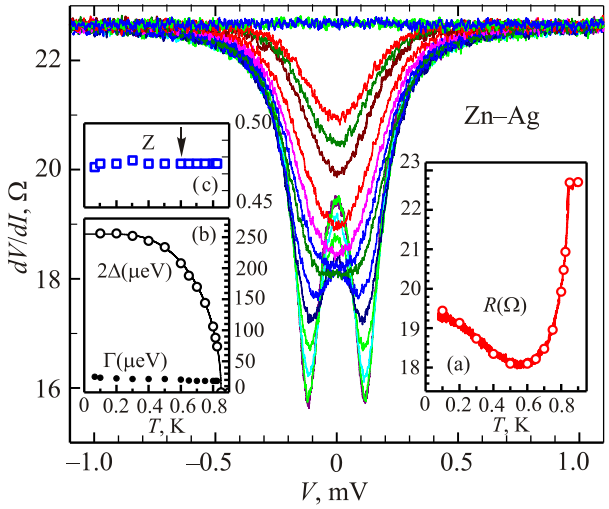

Fig. 1. (Color online) Spectra of a Zn–Ag contact at discrete temperatures from 0.075 to 0.90 K. The insets show as function of temperature T: (a) zero-bias resistance read off the spectra (open symbols) as well as that recorded during the following cool down (solid line); (b) Energy gap 2Δ and Dynes' parameter Γ. The solid line is the theoretical BCS curve adjusted for T_c = 0.85 K and $2\Delta(T \to 0)$ = 255 μeV; (c) Z parameter. The arrow marks the temperature above which Z was kept constant.

3. Discussion

Our main experimental results in Figs. 2–5 confirm earlier observations that S–N contacts have rather similar Z parameters around 0.5 [6–10]. Explanations based on a dielectric tunneling barrier, Fermi-surface mismatch, or diffusive contacts, have to reproduce the very small variation of Z.

The question of a dielectric interface barrier can be resolved most easily. Such a barrier, or its remnants, could be present because we have prepared the contacts at ambient conditions. However, if tunneling would be the dominant mechanism one would expect a much larger variation of Z not only from metal-to-metal combination but also from contact to contact [10]. The experimental data in Figs. 2–5 demonstrate the opposite, therefore $Z_\delta \ll 0.5$ for contacts with $R_N \lesssim 1\,\mathrm{k}\Omega$. We can not exclude that

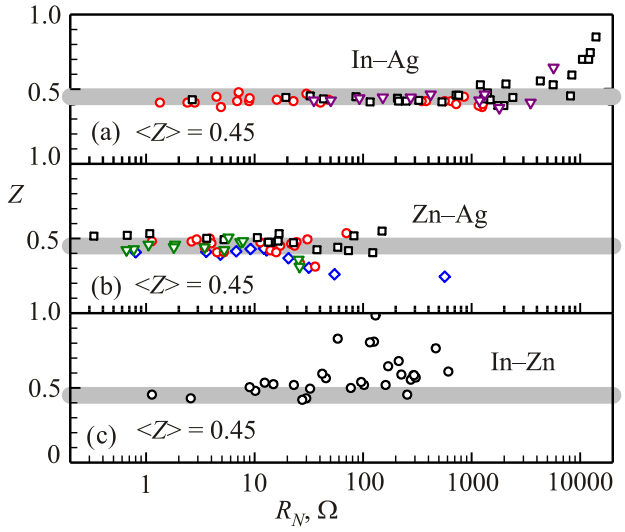

Fig. 2. (Color online) Z parameter of S–N contacts of (a) In–Ag, (b) Zn–Ag, and (c) of S_1–S_2 contacts In–Zn. The In–Ag as well as the Zn–Ag contacts were measured 0.1 K, the In–Zn contacts at 2.5 K to suppress superconductivity in Zn. Different symbols denote measurement series with different sample wires from the same batch. The thick solid lines represent an average $\langle Z \rangle$ = 0.45 with a ±0.05 bandwidth.

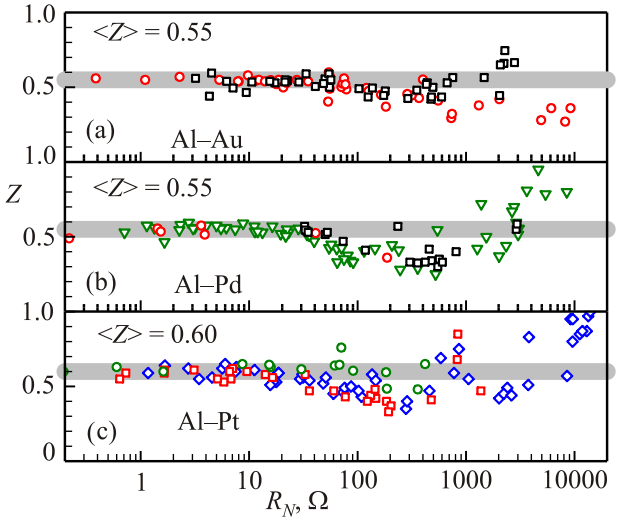

Fig. 3. (Color online) Z parameter of S–N contacts of (a) Al–Au, (b) Al–Pd, and (c) Al–Pt. All contacts were measured at 0.1 K. The thick solid lines indicate the average $\langle Z \rangle$ with a ±0.05 bandwidth.

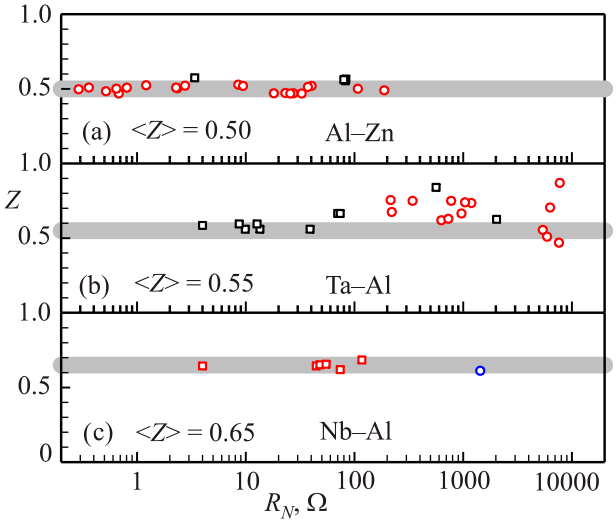

Fig. 4. (Color online) Z parameter of S_1–S_2 contacts of (a) Al–Zn, (b) Ta–Al, and (c) Nb–Al. The Al–Zn contacts were measured in the normal state of Zn around 0.85 K, while the Ta–Al and Nb–Al contacts were measured at 2.5 K or higher to suppress proximity-induced superconductivity in the otherwise normal Al. The thick solid lines indicate the average $\langle Z \rangle$ with a ±0.05 bandwidth.

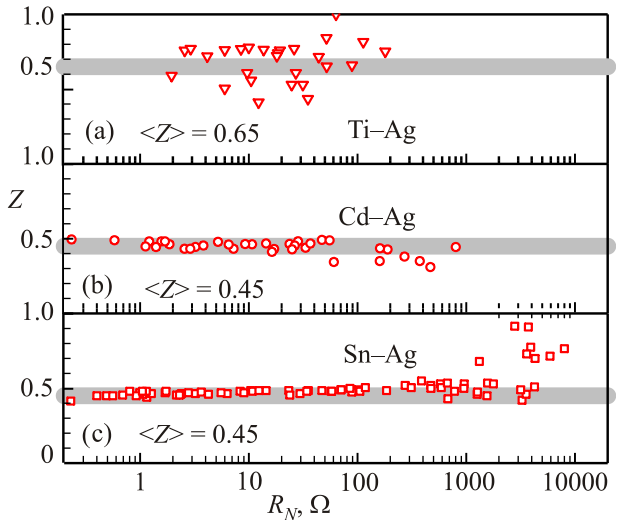

Fig. 5. (Color online) Z parameter of S–N contacts of (a) Ti–Ag, (b) Cd–Ag, and (c) Sn–Ag, measured at 0.1 K The thick solid lines indicate the average $\langle Z \rangle$ with a ±0.05 bandwidth. The Ti–Ag data scatter over more than twice this width.

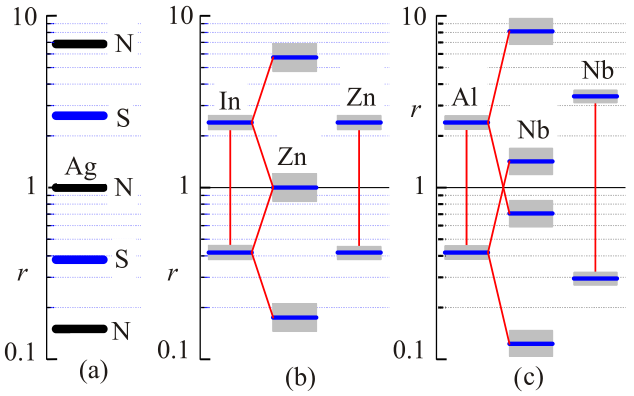

Fig. 6. (Color online) Fermi velocity r (thick horizontal bars) normalized with respect to that of Ag. (a) Fermi-surface mismatch only causes all superconductors (S) to fall into two categories with $r \approx 2.62$ or $r \approx 0.38$, assuming an average $Z \approx 0.50$. In turn all normal metals (N) either have $r \approx 6.85$, 1.00, or 0.16. (b) Fermi velocities of In and Zn derived from In–Ag and Zn–Ag contacts as well as that of Zn calculated from In–Zn junctions. The shaded areas indicate error margins of $\Delta Z = \pm 0.05$. The two ways to derive r of Zn clearly do not match. (c) Likewise the Fermi velocities of Al and Nb are derived from Al–Ag and Nb–Ag contacts, then the velocity of Nb is calculated from Nb–Al contacts.

tunneling plays a role for some of the In–Zn and Ti–Ag contacts which, nevertheless, agree with the lower bound of $Z \approx 0.4 - 0.5$.

The second reflection mechanism, Fermi-surface mismatch, can also not explain the small variation of the Z parameter. Each time we make a new contact, the orientation of the crystallites that form the interface changes, and the Z parameter should change accordingly. Since this is not observed, one should expect that $Z_{FSM} \ll 0.5$ [10].

A second argument against Fermi-surface mismatch comes from the magnitude of Z for inter-related pairs of metals. Take for example Zn–Ag and Zn–Cu contacts. They both have nearly the same $Z \approx 0.45$, that means the Fermi velocity of Ag and Cu would be either 2.39 or 1/2.39 = 0.42 times that of Zn, using $Z = Z_{FSM} = |1 - r| / (2\sqrt{r})$. From Ref. 16 we get Fermi-velocity ratios of 1.16 for the Zn/Ag and 1.32 for the Zn/Cu pair, respectively. These two sets of data do not agree well with each other. The fact that Ag in contact with other superconductors and those superconductors in contact with other normal metals have rather similar $Z \approx 0.5$ would imply the existence of just two groups of superconductors that have $r \approx 2.62$ and $r \approx 0.38$ as well as three groups of normal metals with $r \approx 2.62^2$, $r \approx 1.0$, and $r \approx 0.38^2$ as indicated schematically in Fig. 6(a). However, we have not found any S–N combination with $Z \gtrsim 1$ (velocity ratio $r \gtrsim 2.62^2$ or $r \lesssim 0.38^2$). Therefore, all normal metals would have Fermi velocities near that of Ag, while all superconductors have either $r \approx 2.39$ or $r \approx 0.42$ with respect to Ag. This does not seem plausible.

Consider other combinations between one normal and two superconductors like the Ag, In, and Zn triple. For In/Ag we get from Ref. 16 a velocity ratio of 1.25. But now we can also measure normal Zn in contact with superconducting In. They have the same $Z = 0.45$. Again use Ag as reference in Fig. 6(b). According to the first two experiments on Zn–Ag and In–Ag contacts, Zn and In should have Fermi velocities of either 2.39 or 0.42 times that of Ag. The third experiment with In–Zn contacts indicates that Zn should have a Fermi velocity of 2.39 or 0.42 times that of In, that is 0.42·0.42 = 0.18, 0.42·2.39 = 1.00, or 2.39·2.39 = = 5.72 times that of Ag. This contradicts the In–Ag data even if we allow for an uncertainty of $\Delta Z \approx \pm 0.05$. One can construct similar patterns also for other inter-related metal combinations, like for the Ag, Al, and Nb triple in Fig. 6(c). Thus Fermi-surface mismatch in its common form [2] can not account for the observed Z parameters.

How good is the free electron model for Andreev-reflection spectroscopy? It assumes a spherical Fermi surface and one, two, or three conduction electrons per atom. It describes reasonably well the alkali metals (which we do not use here) but not the transition metals like Nb and Ta or the noble metals Pt and Pd that have rather complex Fermi surfaces [17]. Since electrons from different parts of the Fermi surface contribute to charge transport, it should be rather difficult to identify a specific Fermi velocity in those cases.

Point-contact spectroscopy uses electrical transport properties as information source. Therefore it appears natural to extract an average Fermi velocity from the Bloch–Grüneisen law for the temperature dependence of the electrical resistivity [18]. At high temperatures the resistivity $\rho(T)$ varies linearly with temperature, and does not depend on impurities. The proportionality factor contains the Fermi velocity, the size of the Fermi surface of the conduc-

Table. 1. Bloch–Grüneisen parameters of the various metals. ρ is the electrical resistivity at T = 298 K, Θ_D is the Debye temperature, M is the molar mass, and γ is the Sommerfeld constant of the electronic specific heat. These data have been collected from [21]. v_{BG} is the Bloch–Grüneisen derived velocity Eq. (2) and v_F the free-electron Fermi velocity [16]

Metal	ρ, μΩ·cm	Θ_D, K	M, g/mol	γ, mJ/(mol·K^2)	v_{BG}, arb. units	v_F, Mm/s
Ag	1.59	221	108	0.646	7.35	1.39
Al	2.65	390	27	1.35	4.47	2.02
Au	2.21	178	197	0.69	5.55	1.38
Cd	7.27	221	112	0.687	3.27	1.62
Cu	1.68	310	64	0.695	6.41	1.57
In	8.75	129	115	1.66	3.25	1.74
Nb	14.5	260	93	7.8	0.64	–
Pd	10.54	275	106	9.45	0.61	–
Pt	10.6	225	195	6.54	0.65	–
Sn	11	254	113	1.78	1.43	–
Ta	13.15	225	181	5.87	0.64	–
Ti	42	380	48	3.39	0.54	1.88
Zn	5.96	237	65	0.64	4.59	1.82

tion electrons, the surface area of the Debye sphere, and the strength of the electron–phonon interaction. One can write [19,20]

$$\rho(T) \propto \frac{T}{\gamma v_F^2 \Theta_D^2 ML}, \tag{1}$$

where γ is the Sommerfeld constant of the electronic specific heat, Θ_D is the Debye temperature, M is the molar mass, and L is a length scale that depends on the electron–phonon interaction. Although the Bloch–Grüneisen law describes relative changes of the resistivity quite well [18], it is not commonly used to extract absolute values. However, for our purposes we need only ratios of Fermi velocities, and can get rid of the less well known L's by assuming they are roughly the same for all metals, defining

$$v_{BG} = \sqrt{\frac{T}{\rho(T)\gamma\Theta_D^2 M}} \tag{2}$$

to use instead of the Fermi velocity. Table 1 summarizes the parameters which allow to calculate v_{BG} and thus the velocity ratios $r_{BG} = v_{BG1}/v_{BG2}$ for all investigated metal combinations. We refrain from estimating error margins or how well v_{BG} maps the true v_F and consider it as a number that characterizes the Fermi surface. Note that v_{BG} does not vary much for those metals which have a free-electron v_F given in Ref. 16 except for Ti. v_{BG} is large for metals with a nearly spherical Fermi surface, but small for all others. A rather small v_F of Ti has been noted by Zhang Dianlin *et al.* [22] and Hao Zhu *et al.* [23]. Also Nb is claimed to have a small Fermi velocity [24].

Figure 7 compares theory and experiment. It demonstrates that the Z parameter depends only weakly on the velocity ratio, and that there is a huge background. Therefore another mechanism must be responsible for the main contribution to Z. Assume an independent one represented by Z_0 and write

$$Z^2 \approx Z_0^2 + \alpha \frac{(1-r_{BG})^2}{4r_{BG}} \tag{3}$$

with a weight factor α. The data in Fig. 7 indicate $\alpha \approx 0.1$ so that one can not reliably separate Fermi-surface mismatch even if it would exist.

In summary, all three arguments, i) the little variation of Z from contact to contact, ii) the nonmatching inter-related pairs of S–N junctions, as well as iii) the small variation of Z with the velocity ratio r_{BG} take the same line that Fermi-surface mismatch is not the dominant normal reflection mechanism. Note that arguments i) and ii) apply not only

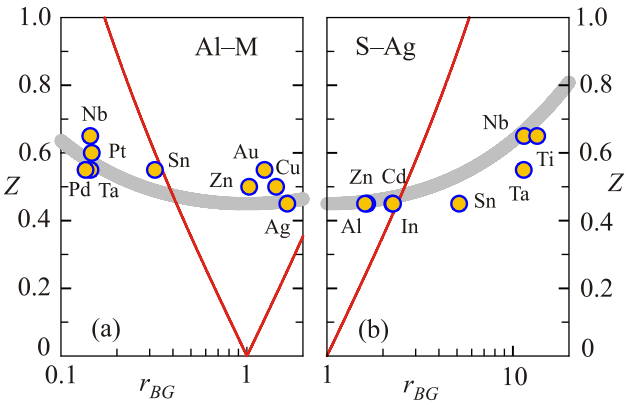

Fig. 7. (Color online) The average Z parameters of contacts between (a) Al and other metals M and (b) superconductors S and Ag as function of their velocity ratio $r_{BG} = v_{BG,M}/v_{BG,\mathrm{Al}}$ and $v_{BG,S}/v_{BG,\mathrm{Ag}}$, respectively. The thin solid line describes the expected Z due to Fermi-surface mismatch [2], the thick solid line is a guide to the eye using $Z^2 = 0.45^2 + 0.1\cdot(1-r_{BG})^2/4r_{BG}$.

to the velocity mismatch but also to the case of the momentum mismatch.

This leaves the third reflection mechanism. Diffusive contacts have $Z \approx 0.55$ in the ideal case of a long channel [3,4]. Thus diffusion would conveniently explain our results, especially the large background Z_0. However, a more realistic short instead of long diffusive channel or a strongly disordered interface should lead to different Z values. We will investigate this possibility elsewhere.

Why is Fermi-surface mismatch absent, or at least strongle suppressed? Electrons as well as Andreev-reflected holes travel through a dielectric tunneling barrier with a certain probability. Those not transmitted are reflected and enhance the contact resistance. The retro-reflected holes that move towards the dielectric barrier can tunnel through with the same probability as the incident electrons. This produces the typical Andreev reflection double-minimum structure of the resistance spectra from which one can extract Z. The same applies to diffusive processes. However, Fermi-surface mismatch works differently because it allows electrons that have corresponding states on the other side to cross the interface and bars all others. That means the transmission probability is either 1 or 0. A retro-reflected hole is not affected again by Fermi-surface mismatch because it has already the right properties to find a corresponding state on the other side. Thus Fermi-surface mismatch affects the absolute value of the contact resistance but not the shape of the Andreev-reflection spectra. Fermi-surface mismatch might play some role in the case of spin-polarized normal metals because there the two spin species have different Fermi surfaces, and the retro-reflected holes flying back to the contact can face conditions that differ from that of the incident electrons.

4. Conclusion

We have found that Fermi-surface mismatch barely affects the normal-reflection part of Andreev reflection. This makes Andreev-reflection spectroscopy unsuitable for measuring relative Fermi velocities of the electrodes, and leaves diffusive transport through the contact, that is elastic scattering at or near the contact interface, as the most probable mechanism to explain the usually observed double-minimum Andreev-reflection anomalies.

Acknowledgments

We thank the Jenny and Antti Wihuri Foundation for financial support.

1. G.E. Blonder, M. Tinkham, and T.M. Klapwijk, *Phys. Rev. B* **25**, 4515 (1982).
2. G.E. Blonder and M. Tinkham, *Phys. Rev. B* **27**, 112 (1983).
3. S.N. Artemenko, A.F. Volkov, and A.V. Zaitsev, *Solid State Commun*. **30**, 771 (1979).
4. I.I. Mazin, A.A. Golubov, and B. Nadgorny, *J. Appl. Phys*. **89**, 7576 (2001).
5. G.T. Woods, J. Soulen, Jr., I. Mazin, B. Nadgorny, M.S. Osofsky, J. Sanders, H. Srikanth, W.F. Egelhoff, and R. Datla, *Phys. Rev. B* **70**, 054416 (2004).
6. Yu.G. Naidyuk, H. v. Löhneysen, and I.K. Yanson, *Phys. Rev. B* **54**, 16077 (1996).
7. Yu.G. Naidyuk and I.K. Yanson, *Point-Contact Spectroscopy*, Springer (2005).
8. E. Tuuli and K. Gloos, *Fiz. Nizk. Temp*. **37**, 609 (2011) [*Low Temp. Phys*. **37**, 458 (2011)].
9. K. Gloos and E. Tuuli, *J. Korean Phys. Soc*. **62**, 1575 (2013).
10. K. Gloos and E. Tuuli, *Fiz. Nizk. Temp*. **39**, 326 (2013) [*Low Temp. Phys*. **39**, 252 (2013)].
11. P.N. Chubov, I.K. Yanson, and A.I. Akimenko, *Fiz. Nizk. Temp*. **8**, 64 (1982) [*Sov. J. Low Temp. Phys*. **8**, 32 (1982)].
12. A. Pleceník, M. Grajcar, Š. Beňačka, P. Seidel, and A. Pfuch, *Phys. Rev. B* **49**, 10016 (1994).
13. Y. de Wilde, T.M. Klapwijk, A.G.M. Jansen, J. Heil, and P. Wyder, *Physica B* **218**, 165 (1996).
14. R.C. Dynes, V. Narayanamurti, and J.P. Garno, *Phys. Rev. Lett*. **41**, 1509 (1978).
15. D.J. Thouless, *Phys. Rev*. **117**, 1256 (1960).
16. N.W. Ashcroft and N.D. Mermin, *Solid State Physics*, Thomson Learning (1976), p. 38.
17. T.-S. Choy, J. Naset, J. Chen, S. Hershfield, and C. Stanton, *A Database of Fermi Surface in Virtual Reality Modeling Language* (vrml). *Bulletin of The American Physical Society* 45(1):L36 42 (2000). http://www.phys.ufl.edu/fermisurface.
18. J.M. Ziman, *Electrons and Phonons*, Oxford, Clarenden Press (1960).
19. D. Varshney, *Supercond. Sci. Technol*. **19**, 685 (2006).
20. K.K. Chaudhary, N. Kauras, and D. Varshney, *J. Phys. Conf. Ser*. **92**, 012075 (2007).
21. http://www.knowledgedoor.com.
22. Zhang Dianlin, Liu Shumei, Jing Xiunian, Luo Jianlin, X.-G. Zhang, Wang Ruju, Kang Ning, Chen Zhaojia, Lu Li, and J.J. Lin, *Int. J. Mod. Phys. B* **19**, 3869 (2005).
23. Hao Zhu, C.A. Richter, Erhai Zhao, J.E. Bonevich, W.A. Kimes, Hyuk-Jae Jang, Hui Yuan, Haitao Li, Abbas Arab, Oleg Kirillov, J.E. Maslar, D.E. Ioannou, and Qiliang Li, *Sci. Rep.* **3**, 1 (2013).
24. H.R. Kerchner, D.K. Christen, and S.T. Sekula, *Phys. Rev. B* **24**, 1200 (1981).